nature physics

LETTERS

https://doi.org/10.1038/s41567-019-0476-x

# Two-dimensional skyrmion bags in liquid crystals and ferromagnets

David Foster[1], Charles Kind[2], Paul J. Ackerman[3], Jung-Shen B. Tai[3], Mark R. Dennis[1,4*] and Ivan I. Smalyukh[3,5,6*]

**Reconfigurable, ordered matter offers great potential for future low-power computer memory by storing information in energetically stable configurations. Among these, skyrmions—which are topologically protected, robust excitations that have been demonstrated in chiral magnets[1–4] and in liquid crystals[5–7]—are driving much excitement about potential spintronic applications[8]. These information-encoding structures topologically resemble field configurations in many other branches of physics and have a rich history[9], although chiral condensed-matter systems so far have yielded realizations only of elementary full and fractional skyrmions. Here we describe stable, high-degree multi-skyrmion configurations where an arbitrary number of antiskyrmions are contained within a larger skyrmion. We call these structures skyrmion bags. We demonstrate them experimentally and numerically in liquid crystals and numerically in micromagnetic simulations either without or with magnetostatic effects. We find that skyrmion bags act like single skyrmions in pairwise interaction and under the influence of current in magnetic materials, and are thus an exciting proposition for topological magnetic storage and logic devices.**

Skyrmions are particle-like topological excitations studied in many condensed-matter systems. For example, some of the earliest reports of liquid crystals (LCs) in the 1800s dealt with chiral phases in cholesterol derivatives extracted from animals, including the so-called 'blue phase'[10–12]. Decades later, these phases were demonstrated to be arrays of fractional skyrmions (also called 'merons'), cubic and hexagonal lattices of double-twist tubes in molecular alignment described by the director field $\mathbf{n}(\mathbf{x})$ with nonpolar head–tail symmetry[7,12]. The rod-like molecules in such a tube are arranged to be parallel to its axis at its centre, twisting radially outwards to form barber-pole-like patterns on concentric cylindrical surfaces (Fig. 1a–c). Elementary full LC skyrmion tubes, with such a 180° radial twist from the centre to the periphery[5,6], exhibit all possible molecular orientations, can be embedded in a uniform far-field background and enjoy topological protection (Fig. 1d,i and Supplementary Fig. 1). In a simply connected manifold, a smooth director structure can always be vectorized and gives a smooth vector configuration (compare Fig. 1c,d with Fig. 1h,i), a process in which the order parameter space changes from $\mathbb{S}^2/\mathbb{Z}_2$ to $\mathbb{S}^2$ (Fig. 1b,g). Therefore, a large number of topologically equivalent solitonic structures have been observed and exhibit similar behaviour in LCs and other condensed-matter systems, such as magnets. The vectorized field can be in two antiparallel orientations and be given topological degrees $Q$ with opposite signs[13]. Here we adopt the convention $Q=-1$ for an elementary full skyrmion in Fig. 1i[14].

The discovery of similar skyrmion configurations in the magnetization field in chiral magnets drives much excitement in spintronics[8]: magnetic skyrmions can be accelerated with a current[15,16], so they might be used to encode data in racetrack memory technology[16–19]. The density of such information could be increased using skyrmions with varying topological degrees (whose distinction is topologically protected). One could consider realizing high-degree skyrmions by introducing an extra π-twist beyond the fundamental full skyrmion, equivalent to placing a skyrmion inside another skyrmion (Fig. 1j). However, this coaxial structure, so-called skyrmionium, has zero topological charge. The process of placing central (anti)skyrmions inside a larger skyrmion, while maintaining axial symmetry, can be iterated to produce configurations with multiple π-twists from the centre to the far-field periphery, called target skyrmions (Fig. 2a). The topological degree of such axial configurations, increasing layers of π-twists, alternates between 0 and −1 due to cancellation from the contribution of adjacent twists, and therefore the inventory of topological degree is not extended. Only fractional and elementary full skyrmions have previously been realized in chiral condensed-matter systems.

Here we report the discovery of stable chiral composite skyrmion bags that can have arbitrary topological degree. We experimentally realize and numerically study them in LCs and in models and micromagnetic simulations of ferromagnets, demonstrating their enhanced stability, and in ferromagnets both without and with the influence of demagnetizing field effects. Using a combination of laser tweezers and videomicroscopy, we experimentally probe pair interaction between skyrmions and skyrmion bags in LCs and demonstrate how their behaviour resembles that in the magnetic counterparts. These high-degree skyrmion configurations may enable a new paradigm-changing approach in encoding information in magnetic data storage, and could lead to electro-optic, microfluidic, nanoparticle transport and display applications dealing with topologically protected multi-stable states of chiral LC matter.

In LCs, multiple π-twist target skyrmions can be generated by iterating the process of stretching a skyrmion with laser tweezers, and then creating an antiskyrmion inside. We have found these configurations to have poor stability and existing only as transient structures. For example, a 6π-twist LC target skyrmion can collapse within 3 min, as illustrated in Fig. 2a and in Supplementary Video 1.

[1]H. H. Wills Physics Laboratory, University of Bristol, Bristol, UK. [2]School of Mathematics, University of Bristol, Bristol, UK. [3]Department of Physics and Soft Materials Research Center, University of Colorado, Boulder, CO, USA. [4]School of Physics and Astronomy, University of Birmingham, Birmingham, UK. [5]Department of Electrical, Computer, and Energy Engineering, Materials Science and Engineering Program, University of Colorado, Boulder, CO, USA. [6]Renewable and Sustainable Energy Institute, National Renewable Energy Laboratory and University of Colorado, Boulder, CO, USA. *e-mail: mark.dennis@physics.org; Ivan.Smalyukh@Colorado.edu

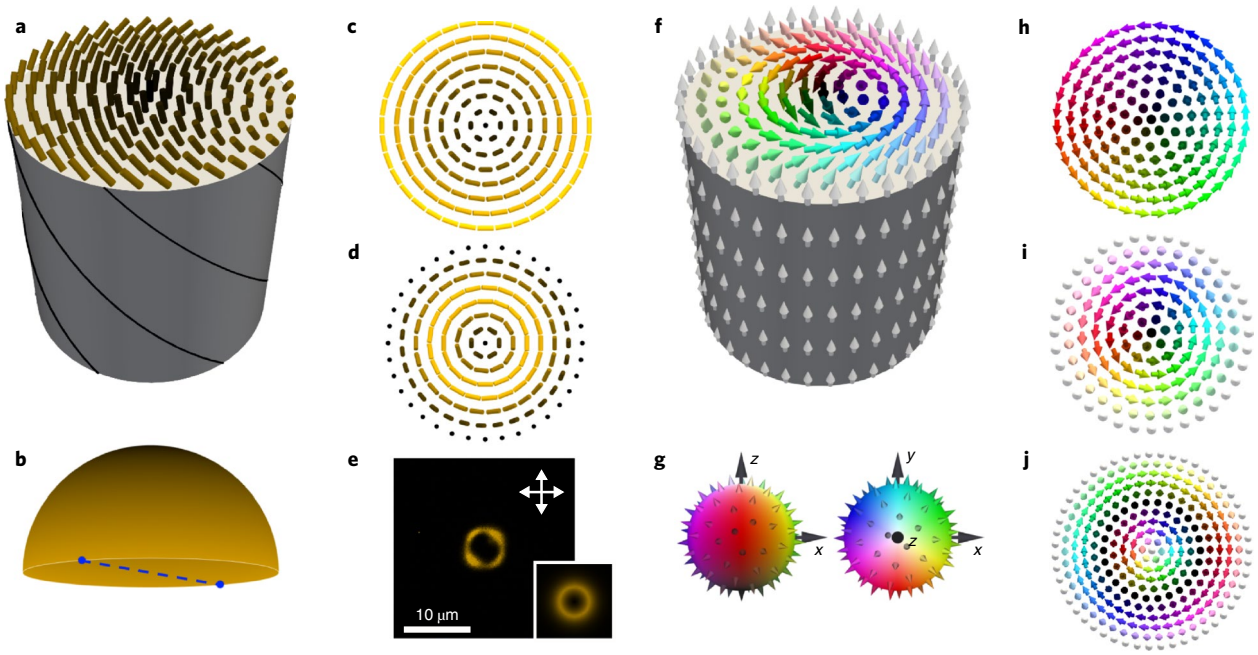


**Fig. 1 | Solitonic structures of a fractional skyrmion, skyrmion and skyrmionium. a**, A translationally invariant quarter-skyrmion tube with **n**(**x**), visualized by rods whose colour is based on their orientations in the $\mathbb{S}^2/\mathbb{Z}_2$ order-parameter space shown in **b**. **b**, The colour scheme for **n**(**x**) in **a**–**e** determined by orientations in $\mathbb{S}^2/\mathbb{Z}_2$, where diametrically opposite points around the base of a hemisphere are identified. **c**,**d**, Top views of a half-skyrmion (**c**) and an elementary full skyrmion (**d**) in the director field. **e**, A polarizing optical micrograph of a LC skyrmion. The computer visualization based on the colour scheme in **b** is shown in the inset. **f**, A translationally invariant skyrmion tube visualized by coloured arrows smoothly decorating **n**(**x**) based on their orientations on the $\mathbb{S}^2$ sphere in **g**. **g**, The Runge colour sphere is used for the vectors in **f**–**j**, with hues and brightness determined by the representation of **n**(**x**) on $\mathbb{S}^2$, viewing from the side and from above. **h**–**j**, Top views of a vector-field half-skyrmion (**h**), full skyrmion (**i**) and skyrmionium (**j**).

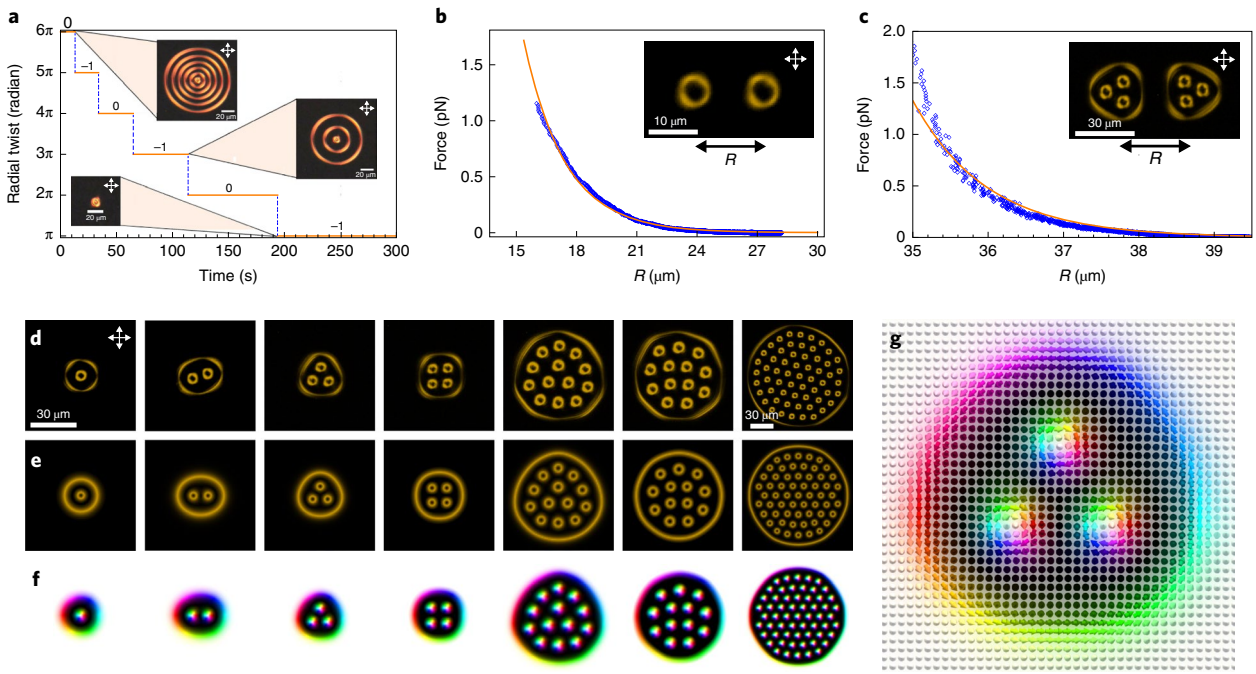


**Fig. 2 | LC skyrmion bag configurations and decay of target skyrmions. a**, A 6π-twist target skyrmion in LCs collapsing to an elementary full skyrmion within 200 s (Supplementary Video 1). The topological degrees (0 or −1) are labelled. **b**, Experimental measurement of the repulsion of two LC skyrmions (points), fitted to the dipole interaction force (Supplementary equation (2)). **c**, Experimental measurement of two repelling *S*(3) LC bags (points), with the fitted dipole interaction (Supplementary equation (2)) as in **b**. The interaction in these two cases has the same asymptotic form as between single skyrmions. **d**, Polarizing optical micrographs of skyrmion bags *S*(1) to *S*(4), two stable conformations of the *S*(13) bag, and the *S*(59) bag. The packing of antiskyrmions inside bags resembles that of hard disks—in particular, the two *S*(13) bag configurations are analogous to the two closest packings of 13 disks[28]. **e**, Computer-simulated counterparts of the skyrmion bags in **d** visualized by colours based on director orientation. **f**, Computer-simulated counterparts of the skyrmion bags in **d** visualized by colours based on vector orientation (Fig. 1g). **g**, A close-up view of a computer-simulated *S*(3) bag visualized by coloured arrows. The experimental data were obtained with the chiral LC 5CB/cholesteryl pelargonate in **a** and ZLI-3412/CB-15 elsewhere.

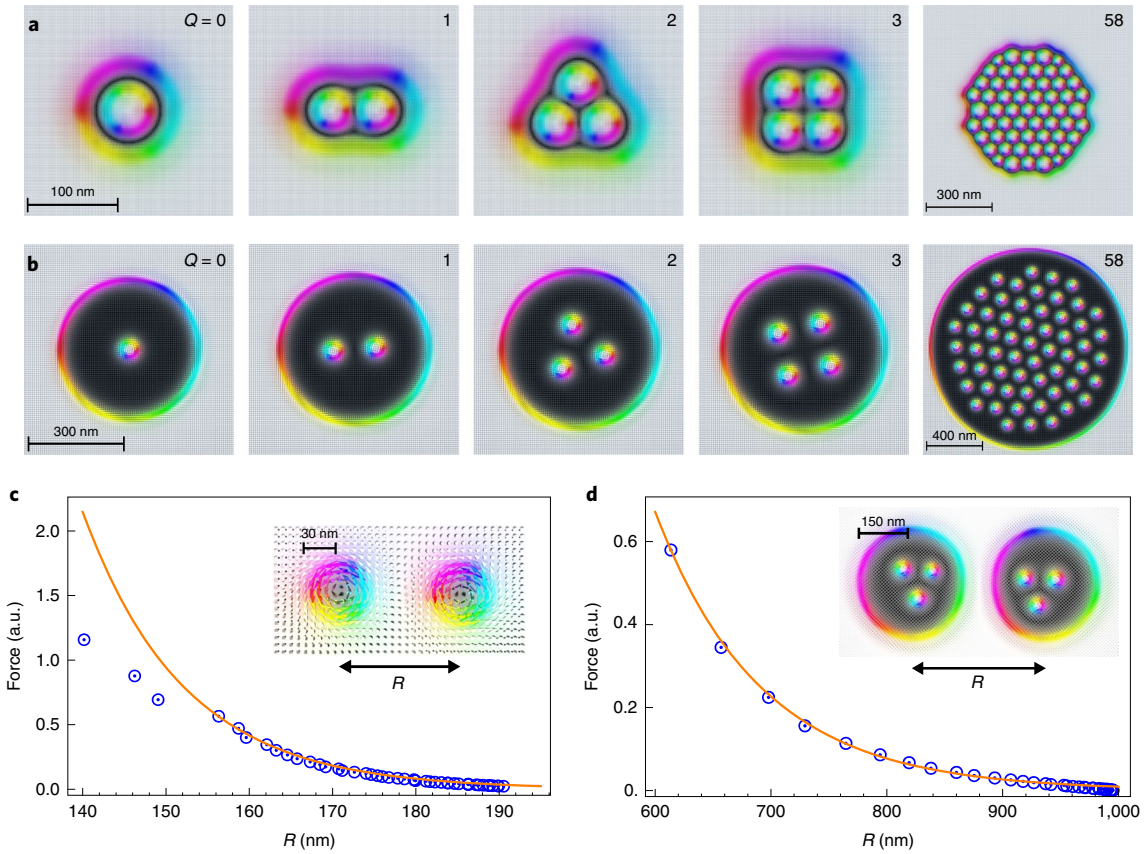


**Fig. 3 | Skyrmion bag configurations in chiral ferromagnets. a**, Magnetic simulations of skyrmion bag configurations in chiral magnets with the topological degree labelled in the top right corner of each panel. Simulations were performed for $J = 7.290\,\mathrm{pJ\,m^{-1}}$, $D = 0.567\,\mathrm{mJ\,m^{-2}}$, saturation magnetization $M_{sat} = 111\,\mathrm{kA\,m^{-1}}$, corresponding to material parameters of FeGe[27], and the applied magnetic field $B = 258\,\mathrm{mT}$. **b**, Simulations similar to those shown in **a**, but accounting for the demagnetizing field, which were implemented using MuMax3. **c**, Dynamical MuMax3 simulation of two magnetic skyrmions repelling (points), with the fitted dipole interaction force (Supplementary equation (2)). **d**, Dynamical MuMax3 simulation of two $S(3)$ magnetic bags repelling (points), with the fitted dipole interaction force (Supplementary equation (2)). In **b**–**d**, the physical parameters used in the simulations are: $J = 20\,\mathrm{pJ\,m^{-1}}$, $D = 0.6\,\mathrm{mJ\,m^{-2}}$, $M_{sat} = 900\,\mathrm{kA\,m^{-1}}$ and uniaxial anisotropy $K_u = 0.56\,\mathrm{MJ\,m^{-3}}$.

The equivalence of the field topology of target skyrmions to an elementary full skyrmion (with an odd number of π-twists) or the uniform state (with an even number of π-twists) is also demonstrated in Supplementary Video 2, where a 2π-twist skyrmionium transforms smoothly to the uniform trivial state.

Unlike the composite skyrmions that occur in the Skyrme model[9], elementary full skyrmions in condensed-matter systems[20] are observed as energy minima due to the inter-skyrmion interaction potential being repulsive and asymptotically dipolar (described in Supplementary Information and Supplementary Figs. 2 and 3), preventing two skyrmions from forming a single composite object. The repulsive force between a pair of interacting LC skyrmions is shown in Fig. 2b. Through this repulsive interaction in a target skyrmion, the central skyrmion contracts due to the accumulative pressure from each exterior skyrmion ring (that is, concentric π-twist), resulting in its poor stability (Supplementary Video 1).

To realize stable arbitrary high-degree skyrmion configurations, we place multiple single antiskyrmions (each with degree +1) in a stretched skyrmion (the outer 'bag') without maintaining axial symmetry, thus forming the skyrmion bags (Fig. 2d). These bags have a wide range of accessible topological degrees and are the first example of stable two-dimensional (2D) composite skyrmions of $|\mathrm{degree}| > 1$ in monochiral materials. The range of possible distinct bag configurations echoes the plethora of nuclei described by different topological degree configurations in the original Skyrme model[9]. We denote such bag configurations of $N_A$ antiskyrmions inside a larger bag skyrmion as $S(N_A)$, which has total topological degree $N_A - 1$. Our experimental observations of large $N_A$ skyrmion bags indicate that they can be stable for an indefinite duration, with the bags with $N_A > 1$ shown in Fig. 2 staying topologically unchanged for more than one year already (contrasting with target skyrmions that disappear within seconds). Skyrmion bags interact with each other like large skyrmions (Fig. 2c).

Numerical simulations of stable skyrmion bags in LCs were performed based on minimizing the Frank–Oseen free-energy functional for a chiral nematic in the one-constant approximation. The energy density is[21]

$$f = \frac{J}{2}\partial_i \mathbf{n} \cdot \partial_i \mathbf{n} + D\mathbf{n} \cdot (\nabla \times \mathbf{n}) + f_{ext} \quad (1)$$

where $J$ is the average elastic constant, $D = 2\pi J/p$ with $p$ the helical pitch of the chiral LC, and $f_{ext}$ describes external field coupling terms and an effective uniaxial anisotropy induced by the boundary conditions of the cell. The simulated skyrmion bags are in excellent agreement with their experimental counterparts (Fig. 2e,f). The topological degrees $Q$ of these complex configurations, as with single skyrmions, can be obtained from the integral

$$Q = \frac{1}{4\pi}\int (\mathbf{n} \cdot \partial_x \mathbf{n} \times \partial_y \mathbf{n})\,\mathrm{d}^2\mathbf{x} \quad (2)$$

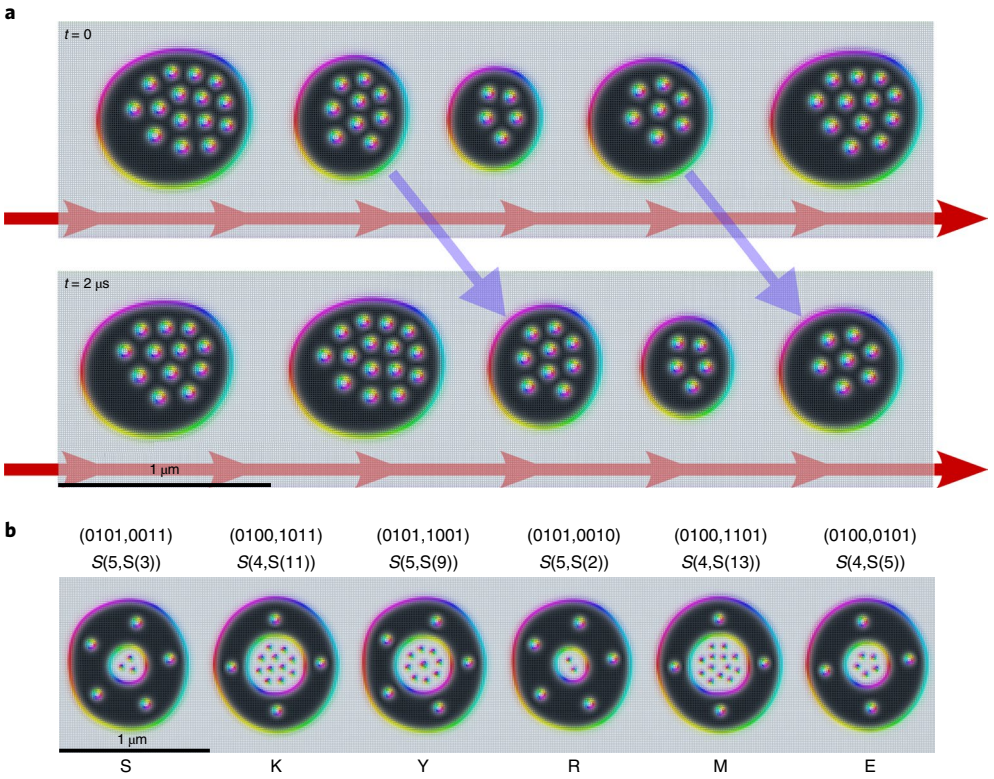


**Fig. 4 | Current-induced motions and data encoding of skyrmion bags. a**, Two frames of a dynamical MuMax3 simulation of a collection of bags in a racetrack being pushed by a current. **b**, A MuMax3 simulation of the word 'SKYRME' using ASCII binary encoding of the alphabet where the outer bag holds the first four bits and the inner bag the next four bits and each full recursive bag represents a single letter and hence eight bits of information. The simulations were performed using the same parameters as for Fig. 3b–d.

By the convention that the arrows are oriented (0, 0, 1) away from the skyrmion centre, an elementary full skyrmion has degree −1 (ref. [14]). Inside a stretched skyrmion, the arrows are oriented (0, 0, −1), and an antiskyrmion placed here has degree +1. Hence, the total degree of an $S(N_A)$ bag is $N_A - 1$ (agreeing with our configurations up to numerical precision). More complex structures with antiskyrmion bags inside skyrmion bags have been experimentally and numerically realized too (Supplementary Fig. 4), giving a net degree $N_A - N_S$, which can in principle be any integer, positive or negative, where $N_S$ is the total number of skyrmions and counting both $N_S$ and $N_A$ includes the both skyrmion and antiskyrmion bags.

We predict that 2D skyrmion bags will also exist in solid-state chiral magnets. The energy density equation (1) is a good description of oriented chiral materials more generally and represents a micromagnetic Hamiltonian (see Methods). We perform dynamical simulations of magnetic skyrmion bags based on the energy density in equation (1) and the Landau–Lifshitz–Gilbert equation using the MuMax3 finite-difference GPU accelerated code[22]. For magnetic systems, $J$ and $D$ describe the exchange and Dzyaloshinskii–Moriya interaction (DMI)[23–26], where $f_{ext}$ incorporates Zeeman coupling, magnetostatic energy and magnetocrystalline anisotropy terms. The skyrmion bags in chiral magnets can be stabilized by an applied magnetic field (Fig. 3a), which leads to the conformational difference compared to their LC counterparts, albeit with identical topology. The effect of including the magnetostatic energy is illustrated in Fig. 3b, where the demagnetizing field acts as an easy-plane anisotropy, effectively expanding the outer bag skyrmion away from the inner antiskyrmions. To assess the potential effects of magnetostatic energy on stability of skyrmion bags, we have used experimental parameters of FeGe (Fig. 3a)[27], as well as a broad range of saturation magnetization and uniaxial anisotropy values (Fig. 3b). The pair interaction of skyrmions and skyrmion bags including the nonlocal magnetostatic effect also shows a dipolar-like dependence at large separations, as shown in Fig. 3c,d. Our findings show that magnetostatic energy tends to further enhance skyrmion bag stability, effectively relieving the tension exerted by the bags on the skyrmions within them (Fig. 3b).

The enhanced stability of skyrmion bags, especially at large $N_A$, can be understood by counting the number of nearest neighbours of each internal antiskyrmion in an optimal packing configuration, much like the mathematical circle packing problem[28] and the packing of magnetic skyrmions in nano discs[29], although in the latter case the outer radius is fixed, constraining the number of interior (anti)skyrmions. In the relaxed state, the radius of the $S(N_A)$ bag grows with $N_A$. At large $N_A$, the number of nearest-neighbour bonds in a hexagonal packing grows to three per skyrmion away from the edges. The energy required to push any two skyrmions together in an equilateral triangle of nearest neighbours is larger than the energy required to push together two skyrmions. Hence, the bags become more stable against decay as $N_A$ increases. Stability is further enhanced by the topology of the antiskyrmion texture. To eliminate such skyrmions within the bag, one needs to nucleate Bloch point defects, which then can eliminate the 2D skyrmions while propagating along their length[30]. The enhanced stability of skyrmion bags with large degrees is also consistent with the fact that the inter-skyrmion spacing approaches that of the hexagonal 2D skyrmion phases in both chiral LCs and magnets (Supplementary Fig. 5). In chiral LCs, a natural inter-skyrmion distance emerges in the 2D hexagonal skyrmion lattice on thermal quenching from the isotropic phase. This is also the case in chiral ferromagnets, where the hexagonal skyrmion $A$ phase is the ground state in certain parameter regions, and the lattice constant is approximately the

helical wavelength[23]. Therefore, the inter-skyrmion distance serves as a good measure of stability in skyrmion bags.

Magnetic skyrmion bags have potential in racetrack memory applications. Conventional proposals for racetrack memory involve encoding bits by separations between elementary full skyrmions, which allows for limited density due to their repulsive interactions. Devices encoding data using the topological degree of skyrmion bags do not have this problem. For example, a train of skyrmion bags, $S(N_1)$, $S(N_2)$, …, encode information by the integer $N_j$, the number of (anti)skyrmions in each bag. Moreover, these bags can be driven along the racetrack by a current. Figure 4a shows the micromagnetic simulation of skyrmion bags being driven by a pulsed current along a racetrack. The average speed of the current-driven skyrmion bags reaches ~1 m s$^{-1}$ at a current density $10^{10}$ A m$^{-2}$ and a duty cycle 20%. There are a variety of ways skyrmion bag configurations can be utilized to store data, including nested bag configurations. For instance, nested double skyrmion bags storing 1 byte of data, by containing 1 to 16 skyrmions in 1 compartment, are shown in Fig. 4b to encode the word 'SKYRME' (see also Supplementary Figs. 4 and 6).

Our experiments and simulations have demonstrated that skyrmion bags are stable, high-degree topological configurations that occur in soft matter and magnetic systems with a range of parameters. In this sense, skyrmion bags play a role for chiral materials echoing the diversity of topological structures used to model atomic nuclei with different baryon numbers. The inventory of multiply-nested bags, however, is clearly broader than their integer topological degrees, suggesting the possibility of ultrahigh-density information storage.

## Online content

Any methods, additional references, Nature Research reporting summaries, source data, statements of data availability and associated accession codes are available at https://doi.org/10.1038/s41567-019-0476-x.

Received: 25 April 2018; Accepted: 18 February 2019;
Published online: 1 April 2019

## References

1. Bogdanov, A. & Yablonskii, D. Thermodynamically stable 'vortices' in magnetically ordered crystals. The mixed state of magnets. *Zh. Eksp. Teor. Fiz* **95**, 178–182 (1989).
2. Cortes-Ortuno, D. et al. Thermal stability and topological protection of skyrmions in nanotracks. *Sci. Rep.* **7**, 4060 (2017).
3. Mühlbauer, S. et al. Skyrmion lattice in a chiral magnet. *Science* **323**, 915–919 (2009).
4. Yu, X. et al. Real-space observation of a two-dimensional skyrmion crystal. *Nature* **465**, 901–904 (2010).
5. Smalyukh, I. I., Lansac, Y., Clark, N. A. & Trivedi, R. P. Three-dimensional structure and multistable optical switching of triple-twisted particle-like excitations in anisotropic fluids. *Nat. Mater.* **9**, 139–145 (2010).
6. Ackerman, P. J., Trivedi, R. P., Senyuk, B., van de Lagemaat, J. & Smalyukh, I. I. Two-dimensional skyrmions and other solitonic structures in confinement-frustrated chiral nematics. *Phys. Rev. E* **90**, 012505 (2014).
7. Duzgun, A. & Selinger, J. V. Comparing skyrmions and merons in chiral liquid crystals and magnets. *Phys. Rev. E* **97**, 062706 (2018).
8. Fert, A., Reyren, N. & Cros, V. Magnetic skyrmions: advances in physics and potential applications. *Nat. Rev. Mater.* **2**, 17031 (2017).
9. Skyrme, T. H. R. A non-linear field theory. *Proc. R. Soc. Lond. A* **260**, 127–138 (1961).
10. Planner, J. Note about cholesterol. *Ann. Chem. Pharm.* **118**, 25–27 (1861).
11. Reinitzer, F. Beiträge zur Kenntniss des Cholesterins. *Monatsh. Chem.* **9**, 421–441 (1888).
12. Hornreich, R. M. & Shtrikman, S. Field-induced hexagonal blue phases in positive and negative dielectric anisotropy systems: phase diagrams and topological properties. *Phys. Rev. A* **41**, 1978–1989 (1990).
13. Senyuk, B. et al. Topological colloids. *Nature* **493**, 200–205 (2013).
14. Yu, X. Z. et al. Transformation between meron and skyrmion topological spin textures in a chiral magnet. *Nature* **564**, 95–98 (2018).
15. Iwasaki, J., Mochizuki, M. & Nagaosa, N. Current-induced skyrmion dynamics in constricted geometries. *Nat. Nanotechnol.* **8**, 742–747 (2013).
16. Fert, A., Cros, V. & Sampaio, J. Skyrmions on the track. *Nat. Nanotechnol.* **8**, 152–156 (2013).
17. Schulz, T. et al. Emergent electrodynamics of skyrmions in a chiral magnet. *Nat. Phys.* **8**, 301–304 (2012).
18. Yu, X. Z. Skyrmion flow near room temperature in an ultralow current density. *Nat. Commun.* **3**, 988 (2012).
19. Zhang, X., Ezawa, M. & Zhou, Y. Magnetic skyrmion logic gates: conversion, duplication and merging of skyrmions. *Sci. Rep.* **5**, 9400 (2015).
20. Melcher, C. Chiral skyrmions in the plane. *Proc. R. Soc. A* **470**, 20140394 (2014).
21. Ackerman, P. J., van de Lagemaat, J. & Smalyukh, I. I. Self-assembly and electrostriction of arrays and chains of hopfion particles in chiral liquid crystals. *Nat. Commun.* **6**, 6012 (2015).
22. Vansteenkiste, A. et al. The design and verification of MuMax3. *AIP Adv.* **4**, 107133 (2014).
23. Nagaosa, N. & Tokura, Y. Topological properties and dynamics of magnetic skyrmions. *Nat. Nanotechnol.* **8**, 899–911 (2013).
24. Dzyaloshinsky, I. A thermodynamic theory of 'weak' ferromagnetism of antiferromagnetics. *J. Phys. Chem. Solids* **4**, 241–255 (1958).
25. Moriya, T. Anisotropic superexchange interaction and weak ferromagnetism. *Phys. Rev.* **120**, 91–98 (1960).
26. Fert, A. & Levy, P. M. Role of anisotropic exchange interactions in determining the properties of spin-glasses. *Phys. Rev. Lett* **44**, 1538–1541 (1980).
27. Takagi, R. et al. Spin-wave spectroscopy of the Dzyaloshinskii–Moriya interaction in room-temperature chiral magnets hosting skyrmions. *Phys. Rev. B* **95**, 220406(R) (2017).
28. Fodor, F. The densest packing of 13 congruent circles in a circle. *Contrib. Algebr. Geom.* **44**, 431–440 (2003).
29. Zhao, X. et al. Direct imaging of magnetic field-driven transitions of skyrmion cluster states in FeGe nanodisks. *Proc. Natl Acad. Sci. USA* **113**, 4918–4923 (2016).
30. Milde, P. et al. Unwinding of a skyrmion lattice by magnetic monopoles. *Science* **340**, 1076–1080 (2013).

## Acknowledgements

D.F. and M.R.D. acknowledge the funding by the Leverhulme Trust Research Programme Grant RP2013-K-009, SPOCK: Scientific Properties Of Complex Knots. The authors also thank A. Bogdanov, M. Gradhand, A. Leonov, A. Saxena, P. M. Sutcliffe and W. Zakrzewski for comments. Research at CU-Boulder (P.J.A., J.-S.B.T. and I.I.S.) was supported by the US Department of Energy, Office of Basic Energy Sciences, Division of Materials Sciences and Engineering, under Award ER46921, contract DE-SC0010305.

## Author contributions

C.K. originally discovered the skyrmion bag configurations. D.F. performed the theoretical analysis, with input from C.K. and M.R.D. P.J.A. and J.-S.B.T. performed the experiments with suggestions from I.I.S. and D.F. J.-S.B.T. performed the numerical analysis in LCs and C.K. in magnets. I.I.S. provided experimental techniques and materials and directed the LC component of the project. P.J.A., J.-S.B.T. and I.I.S. analysed the experimental data. All authors contributed to the preparation of the manuscript.

## Competing interests

The authors declare no competing interests.

## Additional information

**Supplementary information** is available for this paper at https://doi.org/10.1038/s41567-019-0476-x.

**Reprints and permissions information** is available at www.nature.com/reprints.

**Correspondence and requests for materials** should be addressed to M.R.D. or I.I.S.

**Journal peer review information:** *Nature Physics* thanks Ingo Dierking and the other anonymous reviewer(s) for their contribution to the peer review of this work.

**Publisher's note:** Springer Nature remains neutral with regard to jurisdictional claims in published maps and institutional affiliations.

## Methods

**LC experiments and simulations.** *Materials and sample preparation.* To ensure accessibility and a broad impact of our work, pentylcyanobiphenyl (5CB, from EM chemicals) and a low-birefringence nematic mixture ZLI-3412 (EM Chemicals), commonly used and commercially available nematic LC materials, were doped with small amounts of chiral additives, cholesterol pelargonate (Sigma-Aldrich) or CB-15 (EM Chemicals), resulting in left-handed or right-handed chiral nematic LCs. The material parameters of 5CB and ZLI-3412 are listed in Table 1. The helicoidal pitch $p$ of the LC mixture is determined by $p=(\xi\cdot c)^{-1}$, where $c$ is the weight fraction of the additive and $\xi$ is the helical twisting power of the additive. Confining glass substrates were treated with polyimide SE1211 (Nissan Chemicals) to ensure vertical alignment of LCs at the LC/glass interface. Polyimide was applied to substrates by spin-coating at 2,700 r.p.m. for 30 s and then baked for 5 min at 90 °C and then 1 h at 180 °C. LC cells with gap thickness of $d=10$–$20\,\mu$m were produced by sandwiching glass fibre segments in ultraviolet-curable glue. In cells where $d/p\approx 1$, spontaneous and controllably generated structures corresponding to minima of free energy were generated and manipulated using laser tweezers, as detailed below.

*Optical generation and repulsive force measurement of skyrmions and skyrmion bags.* Holographic laser tweezers capable of producing arbitrary patterns of laser light intensity within the LC sample based on an ytterbium-doped fibre laser (YLR-10-1064, IPG Photonics, operating at 1,064 nm) and a phase-only spatial light modulator (P512-1064, Boulder Nonlinear Systems) integrated on an inverted microscope (IX81, Olympus) enabled generation of skyrmions and skyrmion bags and subsequent manipulations[5]. Polarizing optical microscopy and videomicroscopy observations of LC skyrmions were carried out with a CCD (charge-coupled device) camera (Grasshopper, PointGrey Research)[5].

The experimental measurement of the repulsion of two LC skyrmions was performed by producing a configuration of two LC skyrmions with a small separation. We then periodically photographed the evolution of the two-skyrmion configuration. This was then used to evaluate the rate of change of skyrmion separation, which was fitted to the highly damped equation of motion to obtain the interaction force between skyrmions $F_{\rm int}=\xi {\rm d}R/{\rm d}t$, where $R$ is the skyrmion separation and $\xi$ is the viscous drag coefficient determined from analysing Brownian motion of skyrmions[21]. Fitting experimental data with this theoretical result shows a good agreement of the model and experiments (Fig. 2b). The same was done with the $S(3)$ bags (Fig. 2c).

*Numerical simulations of LC skyrmion bags.* For chiral LCs, the Frank–Oseen free-energy density describing the energetic cost of spatial deformations of $\mathbf{n}(\mathbf{x})$ reads

$$\begin{aligned} f &= \frac{K_{11}}{2}(\nabla\cdot\mathbf{n})^2+\frac{K_{22}}{2}(\mathbf{n}\cdot(\nabla\times\mathbf{n}))^2 \\ &\quad +\frac{K_{33}}{2}(\mathbf{n}\times(\nabla\times\mathbf{n}))^2 \\ &\quad +q_0K_{22}\mathbf{n}\cdot(\nabla\times\mathbf{n})+f_{\rm ext} \end{aligned} \tag{3}$$

where $K_{11}$, $K_{22}$ and $K_{33}$ are the splay, twist and bend elastic constants, respectively, and $q_0=\frac{2\pi}{p}$ is the helical wavenumber. By adopting the one-constant approximation (where the bend, twist and splay elastic constants are set equal), equation (3) can be rewritten as equation (1), where $J=(K_{11}+K_{22}+K_{33})/3$ and $D=Jq_0$. The external terms

$$f_{\rm ext}=-\frac{\epsilon_0\Delta\epsilon}{2}(\mathbf{n}\cdot\mathbf{E})^2-\frac{\Delta\chi}{2}(\mathbf{n}\cdot\mathbf{B})^2-W(\mathbf{n}\cdot\mathbf{n}_0)^2 \tag{4}$$

where $\Delta\epsilon$ and $\Delta\chi$ are dielectric and diamagnetic anisotropy of the LC, $\epsilon_0$ is the vacuum permittivity, and $\mathbf{E}$ and $\mathbf{B}$ are the external electric field and magnetic field, respectively. The last term describes an effective anisotropy due to the surface anchoring on the substrates, where $W$ is the anisotropy anchoring constant and $\mathbf{n}_0$ is the easy-axis direction, here coinciding with the far-field LC director. For 2D systems, these external terms can be represented by an effective anisotropy energy term $-\Lambda(\mathbf{n}\cdot\mathbf{n}_0)^2$ and $\Lambda=4.2\,{\rm J\,m^{-3}}$ was utilized in this work. Starting from initial conditions topologically equivalent to the final skyrmion bag configurations, the energy functional as the integral of equation (1) in a 2D plane is minimized until an energy minimum and a stable configuration is found. Details of numerical modelling are described elsewhere[31].

**Table 1 | Material parameters of nematic LCs**

| Material | $K_{11}$ (pN) | $K_{22}$ (pN) | $K_{33}$ (pN) | $J$ (pN) | $D$ (μN m$^{-1}$) | $\xi$ of CB-15 (μm$^{-1}$) | $\xi$ of cholesterol pelargonate (μm$^{-1}$) |
|---|---|---|---|---|---|---|---|
| 5CB | 6.4 | 3 | 10 | 6.5 | 4.1 | 7.3 | −6.25 |
| ZLI-3412 | 14.1 | 6.7 | 15.5 | 12.1 | 7.6 | 6.3 | - |

**Magnetic model and simulations.** *Analytic model.* We follow, for the unit magnetization $\mathbf{n}(\mathbf{x})=\mathbf{M}(\mathbf{x})/|\mathbf{M}(\mathbf{x})|$, the magnetic skyrmion model of ref. [23] using the energy density equation (1), where in this case the external energy is the Zeeman coupling to the external magnetic field. In this simple analytical model, demagnetizing effects are not included. In Supplementary Information, the hedgehog ansatz is applied to configurations satisfying this energy functional (or, equivalently, the LC in the one-constant approximation) to find the profile of a single skyrmion, and their pairwise interaction.

*Micromagnetic simulations.* Throughout, we performed magnetic simulations using the GPU-accelerated micromagnetic simulation program MuMax3[22] with Landau–Lifshitz dynamics in the form

$$\frac{\partial\mathbf{n}}{\partial t}=\hat{\gamma}\frac{1}{1+\alpha^2}(\mathbf{n}\times\mathbf{B}_{\rm eff}+\alpha\ \mathbf{n}\times(\mathbf{n}\times\mathbf{B}_{\rm eff})) \tag{5}$$

where $\hat{\gamma}$ is the gyromagnetic ratio, $\alpha$ is the dimensionless damping parameter, $\mathbf{B}_{\rm eff}$ is the effective field and $\mathbf{n}$ is the magnetization unit vector. The simulations were performed with free boundary conditions. The effective field energy derived from equation (1) includes contributions from exchange, anisotropy, DMI and applied field terms. Specifically, $f_{\rm ext}=-M_{\rm sat}\mathbf{B}\cdot\mathbf{n}-\frac{1}{2}M_{\rm sat}\mathbf{B}_{\rm d}\cdot\mathbf{n}-K_u(\mathbf{n}\cdot\mathbf{n}_0)^2$, where $M_{\rm sat}$ is the saturation magnetization, $\mathbf{B}$ is an external magnetic field normal to the sample plane, $\mathbf{B}_{\rm d}$ is the demagnetizing field, $K_{\rm u}$ is the uniaxial anisotropy constant and $\mathbf{n}_0$ is the easy-axis direction, similar to the far-field orientation.

The simulation geometry is typically a $1{,}024\times1{,}024\,{\rm nm^2}$ square with a cell size of $2\times2\times1\,{\rm nm^3}$ although for finer detail cell sizes of $1\,{\rm nm^3}$ were used. Material parameters of MnSi and FeGe (refs. [27,32]; Supplementary Information and Supplementary Table 1), common chiral magnets, were used and stable structures topologically similar to the ones in LCs were obtained. To further explore the effects of magnetostatic energy (unique for magnets) on skyrmion bag stability, we probed stability of skyrmions for parameters at which these effects are most strongly pronounced. Relatively large values of saturation magnetization were deliberately chosen to explore the effect of the magnetostatic energy, which does not destabilize the configurations even with the exaggerated values chosen here (Fig. 3b). Bags were simulated with bulk DMI in order that LC and micromagnetic models aligned. The material parameters used are included in the figure captions of the simulation results.

To probe interactions, in magnetic simulations, using Mumax3 we numerically approximated a configuration of two relaxed single skyrmions. This configuration was then dynamically evolved and the skyrmions' positions (defined as where the field $\mathbf{n}=(0,0,-1)$) were tracked as a function of time. A similar procedure was performed for the bags, using the centre of the outer bag as the position. The force between skyrmions or skyrmion bags is derived from the rate of change of their absolute separation, using Thiele's equation[33].

We simulate current-induced motion of skyrmion bags through the MuMax3 implementation of Zhang–Li spin-transfer torque with a current in-plane injection geometry through the racetrack[32,34,35]. A current density of $\sim10^{10}\,{\rm A\,m^{-2}}$ leads to a current-induced motion of the skyrmion bags along $+x$. The damping and the non-adiabatic constant of spin-transfer torque were taken to be $\alpha=0.5$ and $\beta=0$. The current is spin-polarized after flowing through the uniform background magnetization direction corresponding to the far-field. The Magnus force, which is often assumed to be proportional to (anti)skyrmion topological degrees, acts on the outer skyrmion bag and inner antiskyrmions in antiparallel directions[34,35]; this skyrmion Hall effect[36] leads the antiskyrmions to cluster in the upper part of the film ($y>0$) and stretch the bags, as can be seen in Fig. 4. The boundaries of the film are sufficiently repulsive, in this regime, to hold the bags close to the midline. We use a pulsing current where in each cycle the current is on for 5 ns and off for 20 ns. This allows the skyrmion bags to relax towards their equilibrium configurations during the off state and mitigates the Magnus force-induced distortion of the bags.

## Data availability

The datasets generated during and/or analysed during the current study are available from the corresponding authors on reasonable request.

## References


31. Tai, J.-S. B., Ackerman, P. J. & Smalyukh, I. I. Topological transformations of Hopf solitons in chiral ferromagnets and liquid crystals. *Proc. Natl Acad. Sci. USA* **115**, 921–926 (2018).
32. Tomasello, R. et al. A strategy for the design of skyrmion racetrack memories. *Sci. Rep.* **4**, 6784 (2014).
33. Koshibae, W. & Nagaosa, N. Theory of skyrmions in bilayer systems. *Sci. Rep.* **7**, 42645 (2017).
34. Fook, H. T., Gan, W. L. & Lew, W. S. Gateable skyrmion transport via field-induced potential barrier modulation. *Sci. Rep.* **6**, 21099 (2016).
35. Iwasaki, J., Mochizuki, M. & Nagaosa, N. Universal current-velocity relation of skyrmion motion in chiral magnets. *Nat. Commun.* **4**, 1463 (2013).
36. Jiang, W. et al. Direct observation of the skyrmion Hall effect. *Nat. Phys.* **13**, 162–169 (2017).